Natural Hazards
and Earth System
Sciences
Discussions

InSAR Technique Applied to the Monitoring of the Qinghai-Tibet Railway

Qingyun Zhang[1,2], Yongsheng Li[2], Jingfa Zhang[2], Yi Luo[2]

[1]Key Laboratory of Earthquake Engineering and Engineering Vibration, Institute of Engineering Mechanics, China
Earthquake Administration, Harbin, 150080, China
[2] Key Laboratory of Crustal Dynamics, Institute of Crustal Dynamics, China Earthquake Administration, 100085, Beijing

Correspondence to: Yongsheng Li (liyongsheng0217@163.com)

Abstract. The Qinghai-Tibet Railway is located on the Qinghai-Tibet Plateau and is the highest altitude railway in the world. With the influence of human activities and geological disasters, it is necessary to monitor ground deformation along the Qinghai-Tibet Railway. In this paper, Advanced Synthetic Aperture Radar (ASAR) (T405 and T133) and TerraSAR-X data were used to monitor the Lhasa-Nagqu section of the Qinghai-Tibet Railway from 2003 to 2012. The data period covers the time before and after the railway was open (total of ten years). This study used a new analysis method (the Full Rank Matrix (FRAM) Small Baseline Subset InSAR (SBAS) time-series analysis) to analyze the Qinghai-Tibet Railway. Before the opening of the railway (from 2003 to 2005), the Lhasa-Nagqu road surface deformation was not obvious; in 2007, the railway was completed and opened to traffic, and the settlement of the railway in the district of Damxung was obvious (20 mm/yr). After the opening of the railway (from 2008 to 2010), the Damxung area had a significant subsidence area, and the north section of the railway was relatively stable. By analyzing the distribution of geological hazards in the Damxung area, the distribution of the subsidence area was found to coincide with that of the geological hazards, indicating that the occurrence of subsidence in the Damxung area was related to the influence of surrounding geological hazards and faults. Overall, the peripheral surface of the Qinghai-Tibet Railway is relatively stable but still needs to be verified with real-time monitoring to ensure that the safety of the railway is maintained.

1 Introduction

Surface deformation monitoring is one of the most advantageous applications of interferometric synthetic aperture radar (InSAR) technology. As far as the research and development of methods and techniques are concerned, InSAR technology has been improved from using a small amount of single-phase SAR data to analyzing time series and processing multiphase and multisource data. Differential InSAR (D-InSAR) technology has been developed on the basis of InSAR technology. In 1989, Grabriel et al. (1989) first used D-InSAR technology to monitor surface deformation, and the level of accuracy was maintained at the centimeter level. In the following decades, D-InSAR technology has been widely used in surface, volcanic deformation, and seismic displacement monitoring. In view of the drawbacks of D-InSAR technology affected by the temporal baseline and spatial displacement, many scholars have proposed new technologies such as joint pixel InSAR

technology, to obtain better settlement detection results(e.g., Xiaolei Lv et al., (2013)). InSAR technology in China developed later but has also achieved good research results. Wang Chao et al. (2000) used radar data to analyze the seismic deformation field and promoted the development of D-InSAR technology in China. Zhenhong Li et al. (2009) improved the atmospheric phase screen (APS) estimation algorithm on the basis of the traditional InSAR short baseline analysis method

5   and proposed the InSAR time series (TS)+atmospheric estimation model (AEM) method to obtain good application results. Li Yongsheng et al. (2015, 2016) proposed new improved methods for identifying errors during phase unwrapping and correcting InSAR technology and advanced sequential InSAR analysis methods, and the study obtained very good results in practical applications.

The Qinghai-Tibet Railway is located on the Qinghai-Tibet Plateau, with a total length of more than 1,100 km, of which 632

10   km are within a permafrost region. This railway is the highest elevation railway in the world and the longest railway crossing over a permafrost region (Han Yufei et al., 2010). The key to the success or failure of the Qinghai-Tibet Railway lies in the roadbed, and the key to the success or failure of the roadbed lies in the permafrost. In particular, under global warming and the impacts of human activities and other factors, the stability of the railway roadbed in permafrost regions is facing great challenges (Wu Qingbai et al., 2008; Liu Yongzhi et al., 2000; Wu Qingbai et al., 2004). Permafrost is very sensitive to the

15   disturbance of external factors; the temperature increase decreases the strength of the frozen soil, the bearing capacity of the frozen soil is reduced, and the ability to resist load is reduced (Wu Ziwang et al., 2005). Moreover, the higher the ice content in the frozen soil is, the greater the settlement after the frozen soil thaws. The Qinghai-Tibet Railway subgrade project adopts the design concept of active cooling (Cheng Guodong et al., 2003), which is currently stable. During the construction of the Qinghai-Tibet Railway, the differential settlement and its countermeasures of the road and bridge transition section in

20   the permafrost region were studied in an experiment (Liu Jiankun et al., 2004), and some countermeasures were proposed to address the differential settlement, but there are many bridges, and the geological condition of the permafrost region is complex (Jin et al. 2008; Zhao et al. 2010). Therefore, the stability of the permafrost under the Qinghai-Tibet Railway is related to the normal operation and safety of the Qinghai-Tibet Railway.

In the past, Qinghai-Tibet Plateau deformation investigation and monitoring mainly rely on field work (Welk 1997; Brown,

25   Hinkel, and Nelson 2000; Ma et al. 2011), but Qinghai-Tibet Plateau areas with harsh natural conditions lead to heavy workloads, and the difficulty of performing the traditional measuring method for analyzing deformation increases substantially (Hu Mingjian et al., 2007; Zhang Xuzhi et al., 2006). Therefore, it is necessary to explore a wide range of unattended, long-term, continuous analyses of the Qinghai-Tibet Railway deformation method. Chao Wang et al. (2017) used the InSAR time-series technique, with high-resolution TerraSAR-X images, to analyze the seasonal deformation

30   features on the Qinghai-Tibet Railway. However, the study area only covers the permafrost region of Beiluhe.

In this paper, the InSAR method using the Full Rank Matrix (FRAM) Small Baseline Subset InSAR (SBAS) proposed by Li Yongsheng (2015) is used to study the deformation of the railway section from Lhasa to Nagqu. Using Advanced Synthetic Aperture Radar (ASAR) and TerraSAR-X data, the crustal deformation information of the Qinghai-Tibet Railway over 10

Natural Hazards
and Earth System
Sciences
Discussions

years (from planning to construction of the railway) was obtained, and the relationship between crustal deformation and surrounding geological disasters was analyzed.

2 Study area

The Qinghai-Tibet Railway is a high-elevation railway that connects Xining (Qinghai Province) to Lhasa (Tibet Autonomous Region) (Figure 1). The Qinghai-Tibet Railway and other national key projects that cross multiple active blocks and faults are vulnerable to earthquakes and other disasters. Monitoring the deformation of these projects is of great significance. InSAR and global positioning systems (GPS) are efficient techniques for monitoring the crustal deformation of Qinghai-Tibet blocks.

The Qinghai-Tibet Railway, highway, transmission line and other national key projects, with their ancillary studies, have the characteristics of strong correlations and continuous long-distance distributions. We need to understand how to use these features to monitor the deformation of a long linear region and reveal the movement of the Qinghai-Tibet Plateau block patterns with the deformations of these major project networks.

The Lhasa-Nagqu part of the railway is located at the bottom of the southern valley of the Nyainqentanglha Mountain in the central part of the Lhasa block. In general, it is north-trending, and the Qinghai-Tibet highway and Lhasa River pass through the area. Figure 2 shows the study area, and the base map is derived from a digital elevation model (DEM). The terrain in the area is undulating, with the Nyainqentanglha Mountain Range in the northwest, a mountainous area in the southeast, and the Yangbajing-Damxung Basin in the middle of the region. The terrain is flat, the Qinghai-Tibet Railway and Qinghai-Tibet Highway pass through the basin, and the vegetation along the railway is rich. Wetlands and low-order regions are widely distributed, and the frozen soil in a long part of the area is rich with ice. The study area is in a midlatitude region, and the land types mainly comprise glaciers, snow, bare rock and other land types. In this area, the Bengco fault lies across the railway; therefore, we also need to study whether the movement of the Bengco fault affects the stability of the railway.

3 Datasets and methodology

3.1 Datasets

The greatest feature of the railway is its long linear engineering, in order to detection and analysis this kind of ground object, we need to meet some requirements. The first is large area coverage because the road direction is not the same everywhere and, in monitoring, the need for a unified reference standard requires large-scale synchronized measurements. Second, to meet the requirements of InSAR technology, such projects need to apply a high-precision InSAR data processing algorithm to carry out high-resolution and fine detection.

The TerraSAR-X data are acquired in stripmap mode, with an incidence angle range of 39 °-40 ° at HH polarization. The potential of the X-band data for detecting higher deformation gradients compared to that of other sensors benefits from high

spatial and temporal resolutions. Nevertheless, the coverage of the stripmap mode data is too small to study long linear engineering. Therefore, in this paper, we use C-band ASAR data and TerraSAR-X data to analyze the stability of the Qinghai-Tibet Railway. We select TerraSAR-X data to verify the accuracy of the ASAR T405 data results over the first corner of the railway in Yangbajain and the ASAR T133 data to analyze the deformation of the railway near the Nagqu area

5 because the ASAR T405 data cannot cover this area completely, and the ASAR T133 data can also verify the accuracy of the ASAR T405 data results over the Nagqu area. The data coverage is shown in Figure 2 with the blue dotted line.

The ASAR T405 data are acquired from August 2003 to September 2010, but there are no data for 2016; therefore, we process the data in three stages (2003-2005, 2007, and 2008-2010). The ASAR T133 data were acquired from November 2007 to August 2010. The TerraSAR-X data were acquired from December 2011 to November 2012.

10 **3.2 Methodology**

To minimize the spatial and temporal decorrelations, we constructed a baseline network (Figure 3) using the following criterion: perpendicular baselines smaller than 200 m and a daytime interval baseline of less than 180 days. Each acquisition node in the network has at least two link pairs, meaning that each node has a minimum number of connections with the other nodes (two are used in this paper).

15 Because of the change in the water vapor content in the atmosphere, phase artifacts in InSAR images caused by path delays, such as radar signal propagations, through the stratified and turbulent atmosphere and ionosphere frequently degrade the interpretability of the phase and correlation signatures of the terrain. The effect of atmospheric delay consists of three parts: 1) the long wavelength effect of the atmosphere, which is similar to the orbit error effect; 2) the short wavelength effect of the atmosphere (i.e., turbulent atmospheric artifacts); and 3) the vertical stratification of the atmosphere, which causes

20 height-dependent refractivity variations. In this paper, the three phase delays are calculated using a network methodology. The methodology estimates the phase delay for each SAR acquisition; then, each atmospheric artifact is simulated. The proposed method can effectively eliminate the atmospheric phase delay in the interferograms.

The specific procedure is as follows:

First, compute all selected SAR data along the vertical baseline and select the main image. Then, generate redundant

25 network interference and generate the SAR raw data for a single look complex (SLC) image. Third, select the appropriate DEM, register the DEM and SAR image, and generate the interference subset. Fourth, resample the data and transform the dataset into a unified coordinate system. Then, use the full rank coherent matrix method to extract the full rank Permanent Scatterers (PS) point, phase unwrapping and orbit error correction. Finally, obtain the data based on the results of deformation rate time series.

4 Results and discussion

To remove the influence of far-field topography and Earth movement around the railway, the image was clipped and retained within a certain area along the railway line. The SAR data before and after the opening of the railway were processed to obtain crustal deformation information along the railway.

5 ### 4.1 InSAR results

The deformation information obtained by ASAR T405 during the construction of the Lhasa-Naqu section of the Qinghai-Tibet Railway from 2003 to 2005 is shown in Figure 5. The crust of this section is relatively stable, there is basically no deformation, and the maximum deformation is approximately 5 mm/yr.

In 2007, the Lhasa-Naqu section of the Qinghai-Tibet Railway was basically completed and opened to traffic. Figure 6
10 shows the deformation information of the line obtained by ASAR T405 in 2007. The area of the line is obviously variable compared with that before the opening of the railway. In the area circled by the elliptical red dotted line, the deformation is large, and the maximum deformation is 20 mm/yr. The operation of the train has a certain impact on the railway, which may because the roadbed bears the weight of the train; therefore, the roadbed is compacted and sinks.

From 2008 to 2010, three years after the smooth operation of the Qinghai-Tibet Railway, the deformation of the line slowed
15 compared with that in 2007 (Figure 7). The main deformation area is consistent with the deformation zone in 2007, mainly in the area of Damxung, which may be due to the geothermal exploitation in the area. By comparing ASAR T405 and ASAR T133, the maximum deformation in this area is 15 mm/yr. However, the deformation in the northern part of the railway is relatively stable.

The overlap area between TerraSAR-X and ASAR is located above Yangbajing, and the deformation field obtained from the
20 two datasets is analyzed. Figure 8(A) indicates that the ASAR acquired the deformation field in the region from 2008 to 2010. There is an obvious uplift area at the corner of the railway from 2008 to 2010, and the maximum cumulative uplift is up to 7 mm/yr. Figure 8(B) shows the deformation field acquired by TerraSAR-X from 2011 to 2013, and the deformation of the uplift area at the corner is obviously smaller and tends to be stable, but there are two subsidence areas in the lower left corner and upper right corner, where the maximum subsidence is 10 mm/yr. The reasons for the subsidence area are
25 analyzed by superposing geological hazards.

For analysis, a section of the railway in Damxung is selected (Figure 9). In 2003-2005, the section of the road surface is basically stable; in 2007, the construction of the railway resulted in a region with a large area of settlement, where the maximum settlement was 20 mm/yr. In 2008-2010, the subsidence area was reduced, and the maximum settlement rate was 10 mm/yr; the surface tended to be stable.

30 Based on the results of the deformation field obtained in 2009-2010, some high-voltage towers along the Lhasa-Naqu railway are analyzed (Figure 10). The results show that different sections of the towers have different drops or lifts. The

maximum lifting capacity of D306 is 20 mm, and the maximum settlement of D269 is 20 mm. Most of the larger variables are located at the corner of the railway and within a section of the line.

4.2 Deformation and hazards

The Qinghai-Tibet Railway runs along the Qinghai-Tibet Plateau and its eastern margin. Under the influence of the uplift of
5   the Qinghai-Tibet Plateau, the topography is generally high in the west and low in the east. The Qinghai-Tibet Railway passes through structural units, such as the modified Nagqu orogenic belt and the Lhasa block. The climatic region of the Qinghai-Tibet Plateau has obvious vertical zoning characteristics, large temperature differences between winter and summer, and strong freeze-thaw weathering, which makes the geological environment along the Qinghai-Tibet Railway and adjacent areas sensitive and conducive to the development and occurrence of geological disasters.

10   In this paper, the upper Yangbajing railway section is selected, and the geological hazard and deformation fields are superimposed (Figure 11). The geological hazards occur mostly in areas with large deformation fields, which are also in the corner along the railway. There is basically no distribution of geological hazard points in the stable area of the deformation field, which shows that the stability of the surrounding geological structure is affected by railway construction and other reasons, resulting in frequent geological hazards. At the same time, to ensure the safe and normal operation of the railway, it

15   is necessary to perform long-term monitoring of the geological and geomorphological conditions around the railway to avoid casualties and economic losses.

4.3 Deformation and Bengco Fault

Garthwaite et al. obtained the deformation field within the Qinghai-Tibet Plateau by using large-scale InSAR technique. The present slip rate of the Bengco fault is 1-4+1 mm/yr. At 90.30° E, the slip rate is 1 mm/yr, which is 40 km west of the
20   rupture zone in 1951 earthquake. At 90.75 °E, the sliding rate is reach 4 mm/yr, which is located in the western part of the rupture zone (Garthwaite et al., 2013). Ryder also uses the InSAR method to estimate the deformation rate of the Bengco fault. The right-lateral slip deformation in 90.4E is approximately 1 ± 1 mm/yr and in 90.9E is approximately 4 ± 1 mm/yr. It is believed that this fracture deformation is mainly caused by the post-earthquake stick-slip effect of two earthquakes in 1951 and 1952 (Ryder, et al. 2014). Taylor et al. studied a series of V-shaped conjugate tectonic belts using InSAR technique. The
25   present slip rates of several tectonic belts in the central and western regions are consistent with GPS results (Taylor et al., 2006).

Using the 32 ASAR image scences between 2004 to 2010 (two adjacent tracks T176 and T405) (figure 12), the same treatment method in the section3.2 was used to obtain the deformation rate of the Bengco fault zone. Three section lines of A-A', B-B', and C-C' are selected in the deformation rate map to analyze the slip rate of the Bengco fault (figure 13). It can
30   be seen from the results that the formation rate of the Bengco area is between 1-3 mm/yr. The east segment is about 2-3 mm/yr, and the west segment is about 1 -2 mm/yr. The intersection of the A-A' section line and the fault is basically the

intersection of the Qinghai-Tibet Railway and the fault-breaking fault zone. From the results of the section deformation rate, it can be seen that the result of the fault slip has little effect on the overall deformation of the railway.

5 Conclusions

We used FRAM SBAS technology to measure deformation rates in the Lhasa Nagqu railway section using 49 ASAR image
5   scenes and 17 TerraSAR-X SAR image scenes collected between August 2003 and November 2012. Due to the lack of data in 2006, we divided the data into five groups. The two datasets can provide detailed deformation information for the Qinghai-Tibet Railway. The main conclusions of this work can be summarized as follows.

(1) Before the opening of the railway, the Qinghai-Tibet Railway deformation was very small and considered stable. During the period of operation after the completion of the railway, the roadbed was relatively unstable during the first two or three
10   years, and different subsidence and uplift zones appeared along the railway. During the later stage, with the accumulation of running time, the road surface gradually became stable, and the shape variations gradually decreased.

(2) The whole railway is relatively stable. The influence of frozen soil around the railway is affected by surface deformation but, in general, this condition is not very serious. However, through the analysis of geological hazards and deformation fields, places where the deformation field changes greatly are more likely to experience geological disasters, and geological
15   disasters and abnormal deformations basically occur at the corner of the railway. Therefore, it is necessary to conduct real-time deformation and geological hazard monitoring along the Qinghai-Tibet Railway.

(3) To continue with the sustainable development of the Qinghai-Tibet Railway, the following analyses are urgently needed. First, the continuous monitoring of ground surface subsidence near the Qinghai-Tibet Railway and surrounding regions must be carried out using a geodetic survey (e.g., GPS and InSAR). Second, the distribution of geological hazards along the
20   Qinghai-Tibet Railway and the regional geological structure need to be analyzed in detail. Finally, for the long-term regional monitoring of InSAR data, the splicing of different orbital data and the processing of massive data are also key problems that need to be solved.

References

Brown, J., Hinkel, K.M., Nelson, F.E.: The Circumpolar Activelayer Monitoring (CALM) Program: Research Designs and
25   Initial Results, Polar Geography, 24 (3), 166–258, doi: 10.1080/ 10889370009377698, 2000.

Chao, W., Zhi, L., Hong, Z., Xinjian, S.: Differential interferometry for the same seismic deformation field of Shangyi - Zhangbei earthquake, Chinese Science Bulletin, 45(23), 2550–2554, 2000.

Gabriel, A.K., Goldstein, R.M., Zebker, H.A.: Mapping small elevation changes over large areas: Differential radar interferometry, Journal of Geophysical Research: Solid Earth (1978–2012), 94(B7), 9183–9191,
30   doi:10.1029/JB094iB07p09183, 1989.

Garthwaite, M.C., Wang, H., Wright, T.J.: Broadscale interseismic deformation and fault slip rates in the central Tibetan Plateau observed using InSAR, Journal of Geophysical Research Solid Earth, 118(9), 5071-5083, doi: 10.1109/TGRS.2009.2019125, 2013.

Guodong, C.: Constructing of the Qinghai-Tibet Railroad using the principle of cooling the roadbed, China Railway Science, 5 24(3): 1–4, 2003.

Huijun, J., Qihao, Yu., Shaoling, W., Lanzhi, L.: Changes in Permafrost Environments along the Qinghai–Tibet Engineering Corridor Induced by Anthropogenic Activities and Climate Warming, Cold Regions Science and Technology, 53, 317–333, doi: 10.1016/j.coldregions.2007.07.005, 2008.

Jiankun, L., Wei-meng, B., Xiaogang, H., Li-ming, B.: Observation and analysis of a new type embankment-bridge 10 transition section in permafrost regions, Journal of Glaciology and Geocryology, 26(6), 800–805, doi: 1000-0240(2004)06-0800-06, 2004.

Lin, Z., Qingbai, W., Sergey, M., Sharkhuu, N.: Thermal State of Permafrost and Active Layer Incentral Asia during the International Polar Year, Permafrost and Periglacial Processes, 21, 198–207, doi: 10.1002/ppp.688, 2010.

Mingjian, H., Ren, W., shiling, T., Xiangfeng, S. Development of drill monitoring instrument for frozen soil settlement, 15 Rock and Soil Mechanics, 28(10), 2215–2218, 2007.

Qingbai, W., Guodong, C., Wei, M.: The impact of climate warming on Qinghai-Tibetan Railroad, Science in China, 47, 122–130, 2004.

Qingbai, W., Tingjun, Z.: Recent permafrost warming on the Qinghai-Tibetan Plateau, Journal of Geophysical Research, 113, 1–22, doi: 10.1029/2007JD009539, 2008.

20 Ryder, I., Wang, H., Bie, L., Rietbrock, A.: Geodetic imaging of late postseismic lower crustal flow in Tibet, Earth & Planetary Science Letters, 404, 136-143, doi: 10.1016/j.epsl.2014.07.026, 2014.

Taylor, M., Peltzer, G.: Current slip rates on conjugate strike‐slip faults in central Tibet using synthetic aperture radar interferometry, Journal of Geophysical Research Solid Earth, 111, B12402, doi:10.1029/2005JB004014, 2006.

Wang, C., Zhengjia, Z., Hong, Z., Qingbai, W., Bo, Z., Yixian, T.: Seasonal deformation features on Qinghai-Tibet railway 25 observed using time-series InSAR technique with high-resolution TerraSAR-X images, Remote Sensing Letters, 8(1), 1-10, doi: org/10.1080/2150704X.2016.1225170, 2017.

Wei, M., Yanhu, M., Qingbai, W., Zhizhong, S., Yongzhi, L.: Characteristics and Mechanisms of Embankment Deformation along the Qinghai–Tibet Railway in Permafrost Regions, Cold Regions Science and Technology, 67, 178–186, doi: 10.1016/j.coldregions.2011.02.010, 2011.

30 Welk, J.E.: Railway Crossing Collision Avoidance System, U.S. Patent, 5, 699-986, 23, 1997.

Xiaolei, L, Yazici, B., Bennett, V., Zeghal, M., Abdoun, T.: Joint Pixels In SAR for Health Assessment of Levees in New Orleans, Geo-Congress, 231, 279–288, 2013.

Xuzhi, Z., Xinghua, W. Deformation characteristics of culverts in permafrost regions of Qinghai-Tibet Railway, Hydrogeology & Engineering Geology, 2, 55–58, 2007.

Yufei, H., Xiaogang, S., Xinjian, S., Chunyan, Q., Chisheng, W., Limin, G., Guifang, Z., Yunhua, L.: Deformation monitoring of Changbaishan Tianchi voleano using D-InSAR technique and error analysis, Chinese journal of geophysics, 53(7), 1571–1579, 2010.

5 Yongsheng, L. Surface Deformation Co-seismic and Post-seismic Activity Constrained by Advanced InSAR Time Series Analysis, Institute of Engineering Mechanics,China EarthquakeAdministration, Harbin, 2014.

Yongsheng, L., Jingfa, Z. Yi, L., Wenliang, J., Zhimin, L. Monitoring of Surface Deformation In Dangxiong Using Time Series Analysis Techniques, Journal of Applied Geodesy, 6(3-4), 215-220, 2010.

Yongsheng, L., Yunfeng, T., Zhenhong, L., Jingfa, Z., Yi, L., Wenliang, J.: Measurement ofsubsidence in the yangbajing geothermal fields, tibet, from terrasar-x insartime series analysis. International Journal of Digital Earth, International Journal

10 of Digital Earth, 9(7), 697-709, 2016.

Yongzhi, L., Qingbai, W., Jianming, Z.: Study on ground temperature field in permafrost regions of Qinghai-Tibet Plateau, Highway, 2, 4–8, 2000.

Zhenhong, L., Fielding, E.J., Cross, P.: Integration of In SAR time-series analysis and water-vapor correction for mapping postseismic motion after the 2003 Bam (Iran) earthquake, Geoscience and Remote Sensing, 47(9), 3220–3230, 2009

15 Ziwang, W., Yongzhi, L.: Frozen soil foundation and engineering construction, Beijing: The Ocean Publishing Company, 142–146, 2005.

20 **Figure 1. Qinghai-Tibet Railway**
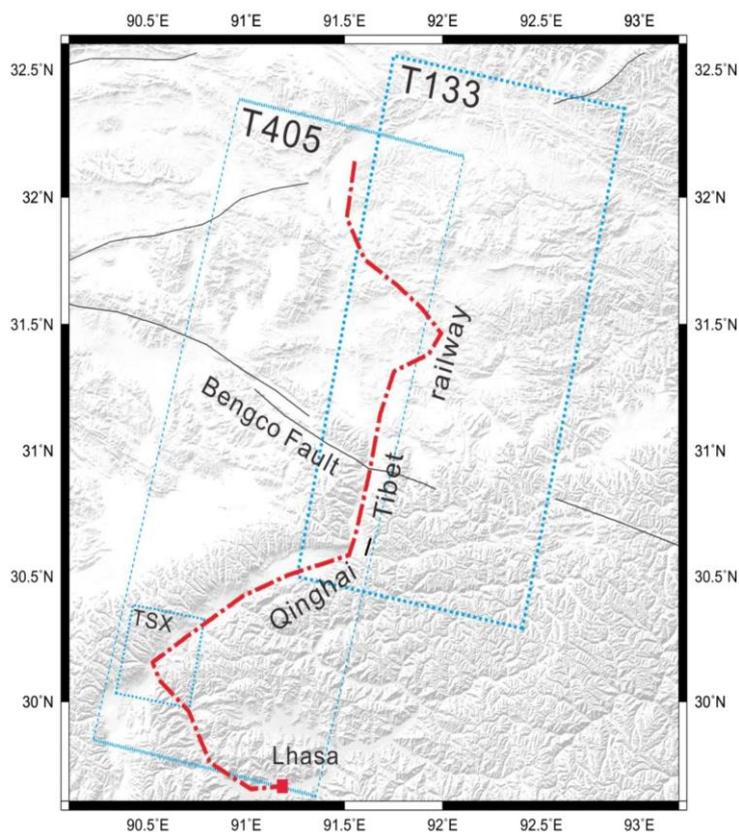
Figure 2. Study area and the distribution of the SAR imagery. The blue dotted line shows the extents of the ASAR and TerraSAR-X images. The red dotted line shows the railway. The black line shows the main fault in this area.
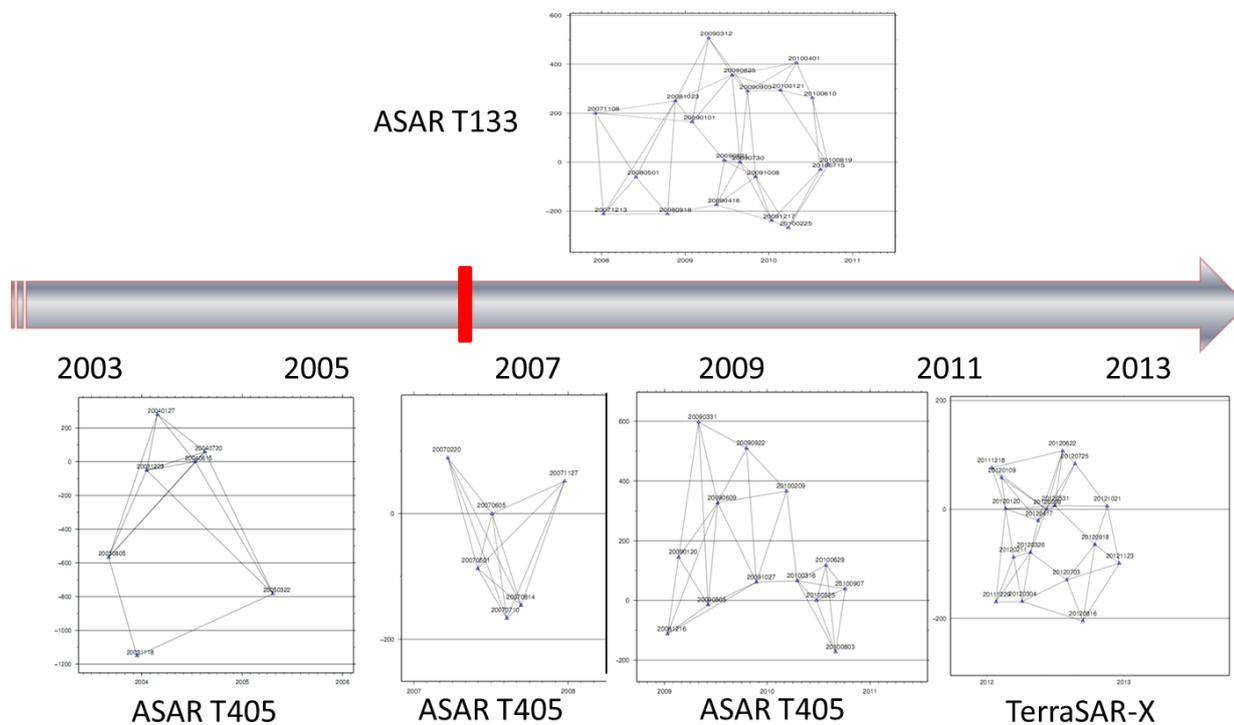
Figure 3. Temporal and perpendicular baselines for the interferograms used in this study. Different graphs represent the baselines of different data generated during different time periods.
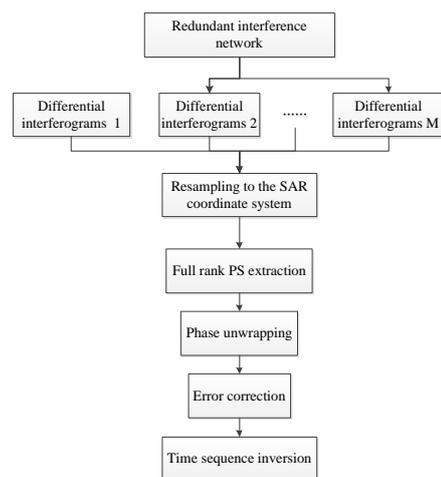
5   Figure 4. Process flow
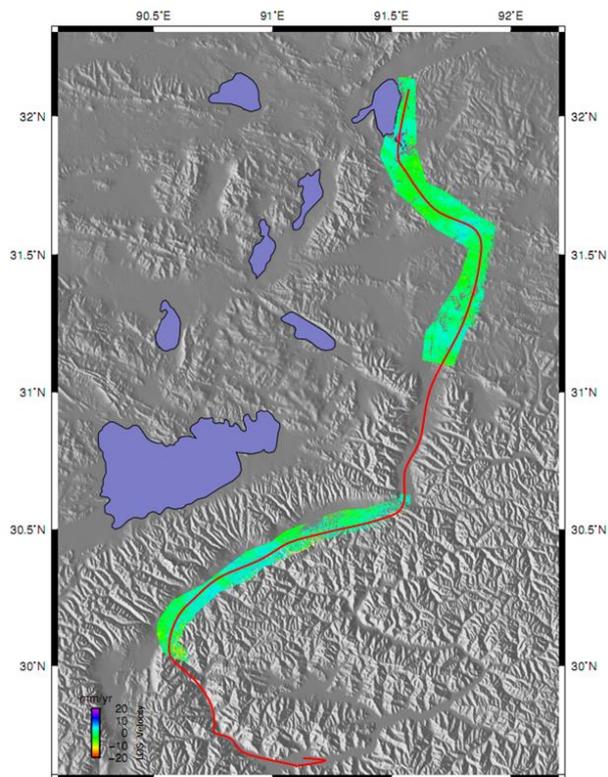
Figure 5. ASAR T405 results for the Lhasa-Naqu section of the Qinghai-Tibet Railway between 2003 and 2005. The red line represents the railway.
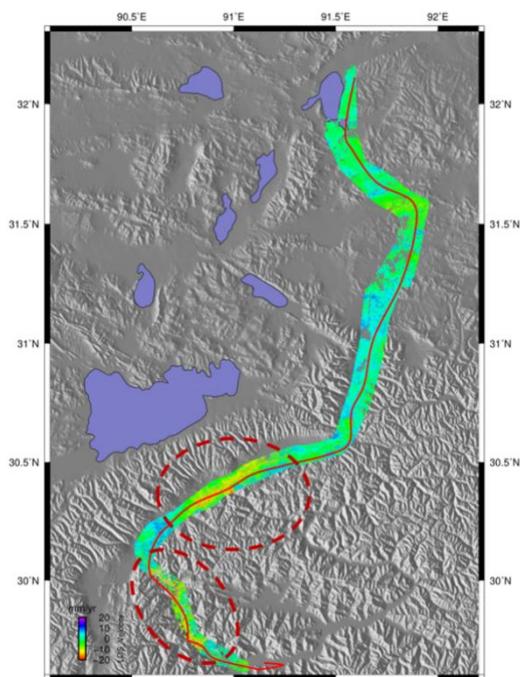
Figure 6. ASAR T405 results for the Lhasa-Naqu section of the Qinghai-Tibet Railway in 2007. The red line represents the railway. The elliptical red dotted line represents the region of large deformation.
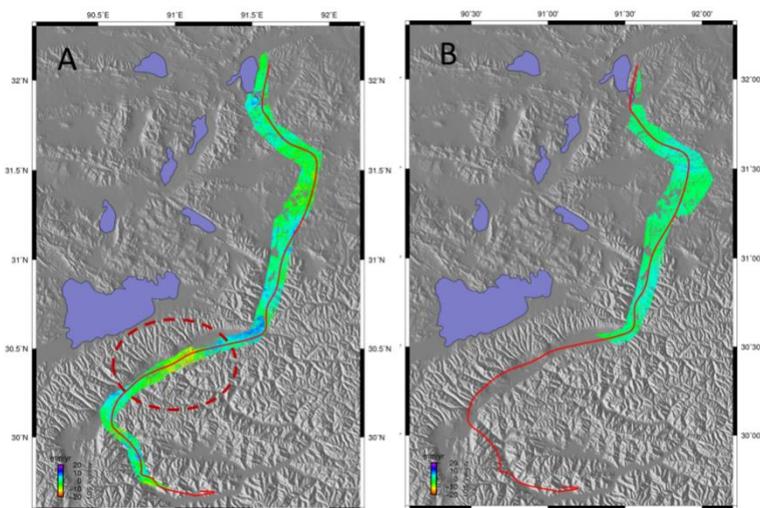
5   **Figure 7. Deformation maps within three years after operation of the railway. (A) The data are ASAR T405 ranging from 2008 to 2010. (B) The data are ASAR T133 from 2008 to 2010. The red line represents the railway.**
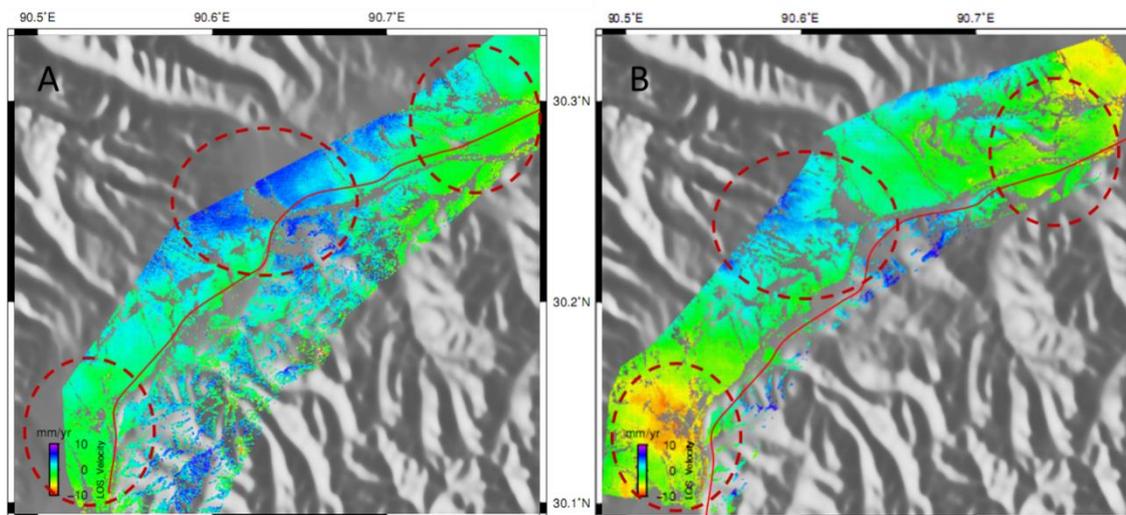
Figure 8. The deformation maps of the overlap area of the TerraSAR-X and ASAR data. (A) The ASAR T405 data range from 2008 to 2010. (B) TerraSAR-X data range from 2011 to 2012.
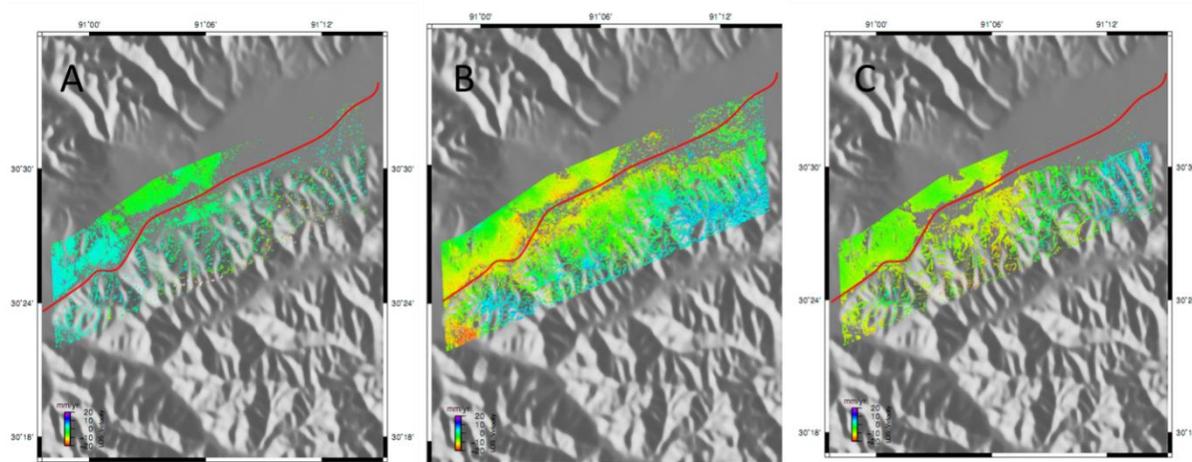
5   **Figure 9. The deformation maps of the railway sequence changes from 2003 to 2010 in the Damxung section.**
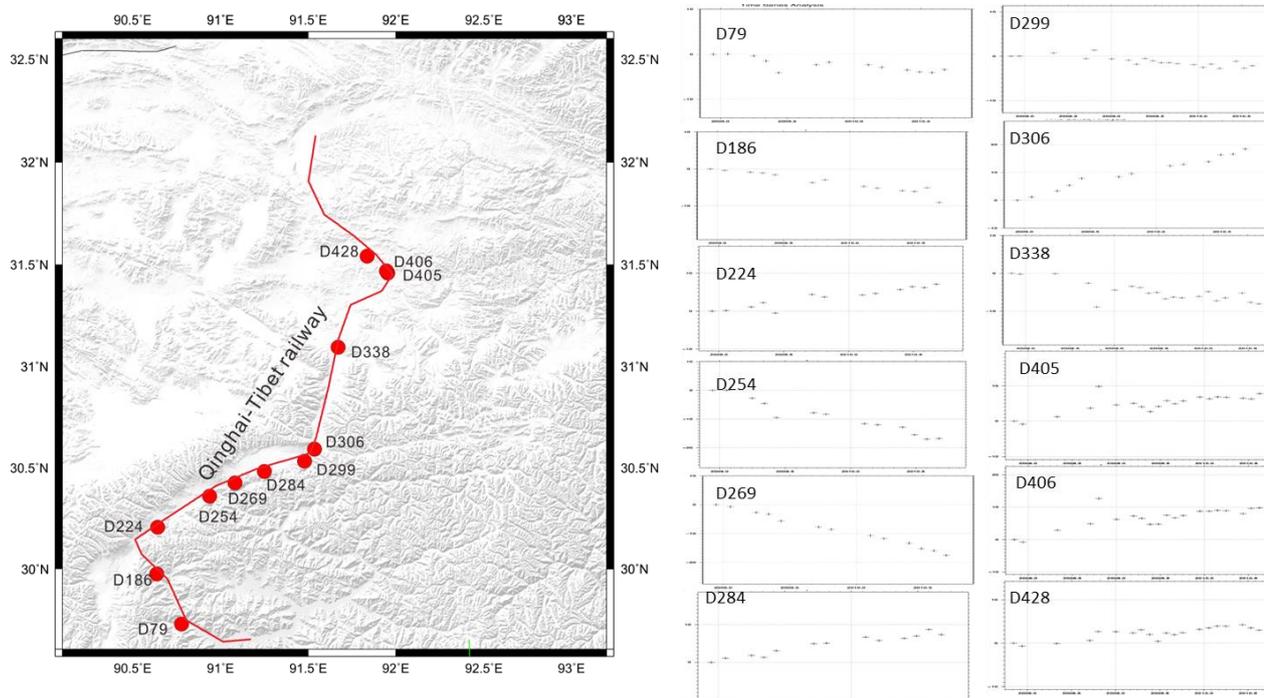
Figure 10. Deformation of a high-voltage power tower. (A) The location of the power tower. (B) The sequence of the deformation characteristics of the power tower.
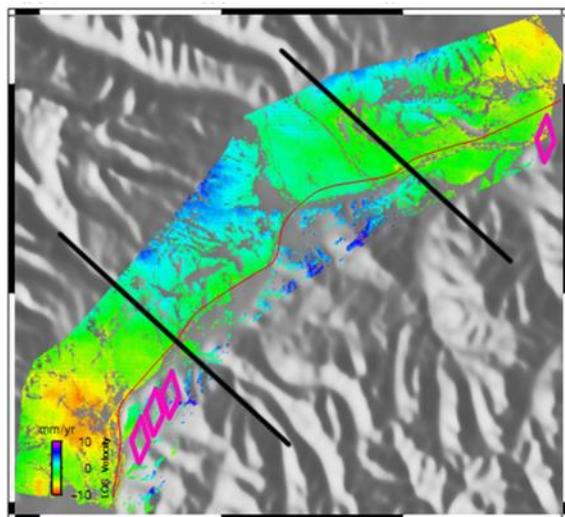
5   **Figure 11. Deformation and hazards. The magenta rhombi show the geological hazard points.**
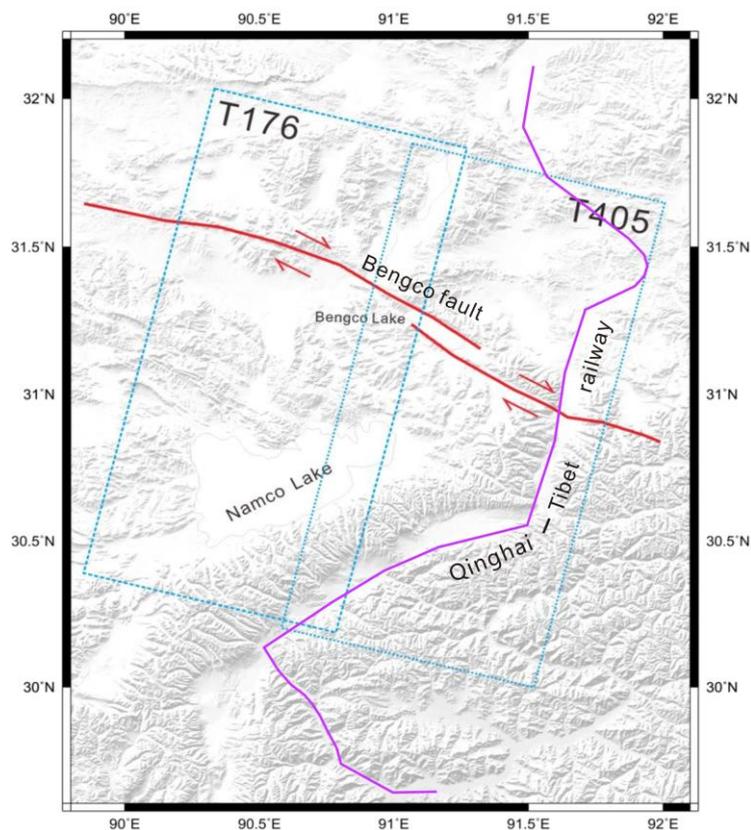
Figure 12. Bengco fault and the distribution of the SAR imagery. The blue dotted line shows the extents of the ASAR images. The red line shows the Bengco fault. The purple line shows the railway.
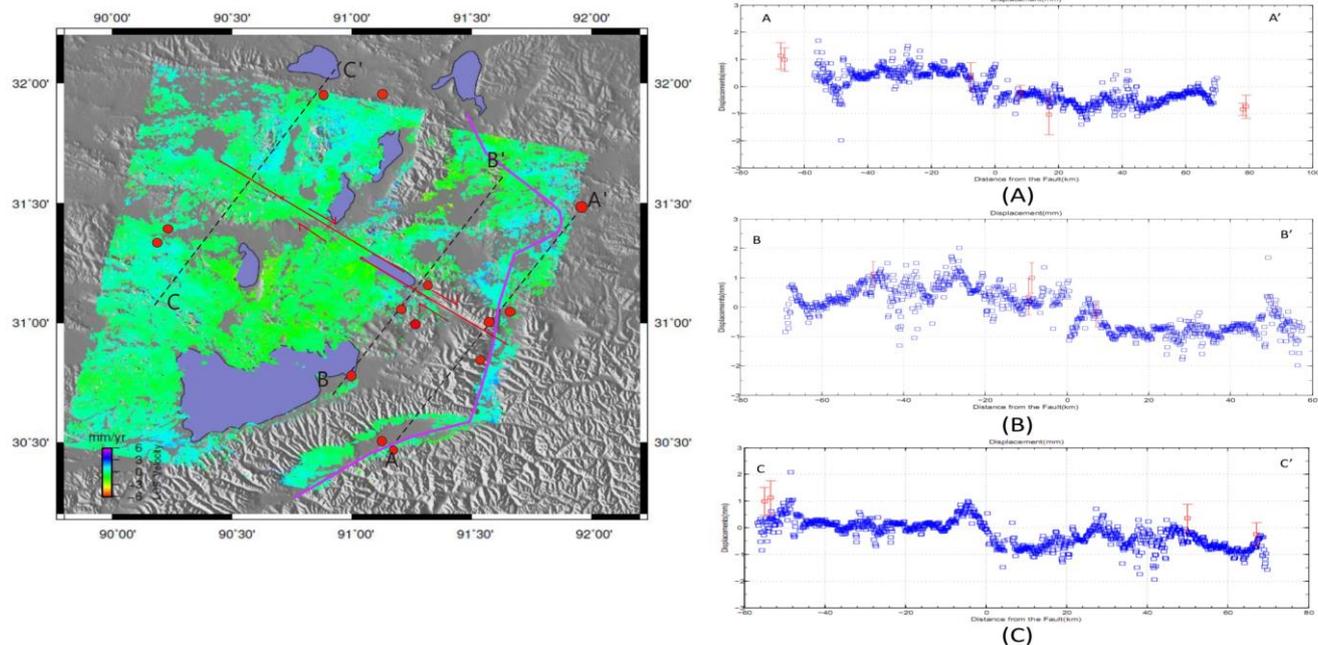
Figure 13. Bengco fault slip rate. The red line shows the Bengco fault. The purple line shows the railway. The red circle shows the GPS location. The black dotted line shows the section lines of Bengco fault. The purple line shows the highway. The left figure shows the Bengco fault slip rate. The right figure shows the detailed information on section lines.